

Constraining the Preferred-Frame α_1, α_2 parameters from Solar System planetary precessions

L. Iorio

Ministero dell'Istruzione, dell'Università e della Ricerca (M.I.U.R.)-Istruzione
Fellow of the Royal Astronomical Society (F.R.A.S.)
Viale Unità di Italia 68, 70125, Bari (BA), Italy

May 25, 2018

Abstract

Analytical expressions for the orbital precessions affecting the relative motion of the components of a local binary system induced by Lorentz-violating Preferred Frame Effects (PFE) are explicitly computed in terms of the PPN parameters α_1, α_2 . Preliminary constraints on α_1, α_2 are inferred from the latest determinations of the observationally admitted ranges $\Delta\dot{\omega}$ for any anomalous Solar System planetary perihelion precessions. Other bounds existing in the literature are critically reviewed, with particular emphasis on the constraint $|\alpha_2| \lesssim 10^{-7}$ based on an interpretation of the current close alignment of the Sun's equator with the invariable plane of the Solar System in terms of the action of a α_2 -induced torque throughout the entire Solar System's existence. Taken individually, the supplementary precessions $\Delta\dot{\omega}$ of Earth and Mercury, recently determined with the INPOP10a ephemerides without modeling PFE, yield $\alpha_1 = (0.8 \pm 4) \times 10^{-6}$ and $\alpha_2 = (4 \pm 6) \times 10^{-6}$, respectively. A linear combination of the supplementary perihelion precessions of all the inner planets of the Solar System, able to remove the a-priori bias of unmodelled/mismodelled standard effects such as the general relativistic Lense-Thirring precessions and the classical rates due to the Sun's oblateness J_2 , allows to infer $\alpha_1 = (-1 \pm 6) \times 10^{-6}, \alpha_2 = (-0.9 \pm 3.5) \times 10^{-5}$. Such figures are obtained by assuming that the ranges of values for the anomalous perihelion precessions are entirely due to the unmodeled effects of α_1 and α_2 . Our bounds should be improved in the near-mid future with the MESSENGER and, especially, BepiColombo spacecrafts. Nonetheless, it is worthwhile noticing that our constraints are close to those predicted for BepiColombo in two independent studies. In further ded-

icated planetary analyses, PFE may be explicitly modeled to estimate α_1, α_2 simultaneously with the other PPN parameters as well.

PACS: 04.80.-y; 04.80.Cc; 04.50.Kd; 96.30.-t; 95.10.Eg; 95.10.Km

Keywords: Experimental studies of gravity; Experimental tests of gravitational theories; Modified theories of gravity; Solar system objects; Orbit determination and improvement; Ephemerides, almanacs, and calendars

1 Introduction

The invariance of the currently accepted laws of physics under Lorentz transformations of the spacetime degrees of freedom [1] is one of the most far-reaching ingredients of our vision of the physical reality. To date, it is routinely corroborated with the greatest accuracy in the high-energy realms of particle physics [2]. The current level of confidence we have on its validity in gravitational physics [3] is relatively less satisfactory because of the challenges in accurate experiments involving gravity [4].

Modified models of the gravitational interaction encompassing violations of the Lorentz symmetry arise in several theoretical scenarios [5–7] such as, e.g., vector-metric theories [8], Tensor-Vector-Scalar (TeVeS) theories [9], Einstein-Æther theories [10–14], MOND [15–18], Hořava-Lifshitz-type theories [19–23], supersymmetric field theories [24, 25], Standard Model Extensions (SME) [26–30]. They predicts several Preferred Frame Effects (PFE) due to the existence of a putative Preferred Frame (PF) which might be singled out by, e.g., the Universe matter distribution.

In the framework of the Parameterized Post-Newtonian (PPN) formalism, Preferred Frame Effects (PFE) are phenomenologically taken into account by the PPN parameters $\alpha_1, \alpha_2, \alpha_3$ [8]. Since α_3 is also related to possible violations of the matter-energy conservation and is very accurately constrained down to a $\approx 10^{-20}$ level from pulsar acceleration data [31], it will be neglected in the following. However, caution is required in straightforward extension of strong-field constraints to weak-field scenarios: α_3 will be the subject of a forthcoming dedicated paper. For an overall overview on the present-day constraints on all the PPN parameters, see [4]. As far as α_1, α_2 are concerned, see also the discussion in Section 4; at present, they are constrained at $\approx 10^{-4}$ (α_1), $\approx 10^{-7}$ (α_2) level by a variety of approaches.

In this paper, we intend to preliminarily explore a different approach with respect to those usually followed so far¹ in constraining both α_1 and α_2 .

¹See, e.g., [4] and references therein.

The plan of the work is as follows. In Section 2 we work out the α_1, α_2 Hamiltonians. They are the basis for perturbatively calculating the averaged orbital precessions of the relative motion of the binary's components in Section 3 by using the Lagrange planetary equations. The resulting analytical formulas are exact in the sense that no a-priori simplifying assumptions about the PF velocity and the orbital geometry are made. In Section 4, after critically discussing the constraints on α_1, α_2 existing in literature, we use the latest determinations of the orbital motions of some planets of the Solar System to preliminary infer bounds on both α_1 and α_2 . More specifically, we compare our analytical predictions with the latest ranges of values for any conceivable anomalous perihelion precessions; since the latter ones are statistically compatible with zero, we are able to obtain upper bounds on α_1, α_2 . In doing that, we assume that the supplementary precessions are entirely due to PFE, not modelled in the dynamical theories fitted by the astronomers to the data. In other words, we actually test PFE theories departing from general relativity in at most α_1, α_2 . Nonetheless, it turns out that our constraints are close to those independently predicted for the future BepiColombo mission by simultaneously estimating α_1, α_2 along with other PPN parameters from simulated data [32, 33]. Section 5 summarizes our findings.

2 The perturbing Hamiltonians

Let us consider a local binary system of total mass $M = m_A + m_B$. Let \mathbf{r}_{CM}^0 be the position vector of the system's center of mass (CM) with respect to the origin of the PF. Thus, we can write

$$\mathbf{r}_A^0 = \mathbf{r}'_A + \mathbf{r}_{\text{CM}}^0 = -\frac{m_B}{M}\mathbf{r} + \mathbf{r}_{\text{CM}}^0, \quad (1)$$

$$\mathbf{r}_B^0 = \mathbf{r}'_B + \mathbf{r}_{\text{CM}}^0 = \frac{m_A}{M}\mathbf{r} + \mathbf{r}_{\text{CM}}^0 \quad (2)$$

where the index $'$ refers to the CM frame; the position vector of m_B with respect to m_A is $\mathbf{r} = \mathbf{r}_B^0 - \mathbf{r}_A^0$ and $\hat{\mathbf{r}} = \mathbf{r}/r$ is its unit vector; in the following, a hat symbol will always denote unit vectors. It follows

$$\mathbf{v}_A^0 = -\frac{m_B}{M}\mathbf{v} + \mathbf{w}, \quad (3)$$

$$\mathbf{v}_B^0 = \frac{m_A}{M}\mathbf{v} + \mathbf{w}, \quad (4)$$

where \mathbf{w} is the PF velocity of the CM.

At post-Newtonian level, the PFE two-body reduced² Lagrangian consists of the sum of the following terms [34–37]

$$\mathcal{L}_{\alpha_1} = -\frac{\alpha_1 GM}{2c^2 r} (\mathbf{v}_A^0 \cdot \mathbf{v}_B^0), \quad (5)$$

$$\mathcal{L}_{\alpha_2} = -\frac{\alpha_2}{\alpha_1} \mathcal{L}_{\alpha_1} + \tilde{\mathcal{L}}_{\alpha_2}, \quad (6)$$

with

$$\tilde{\mathcal{L}}_{\alpha_2} \doteq -\frac{\alpha_2 GM}{2c^2 r} (\mathbf{v}_A^0 \cdot \hat{\mathbf{r}}) (\mathbf{v}_B^0 \cdot \hat{\mathbf{r}}), \quad (7)$$

where G is the Newtonian constant of gravitation, and c is the speed of light in vacuum. For a comparison with the bounds on α_2 inferred by Nordtvedt [34, 35], we notice that he adopted a nonstandard normalization: $\alpha_2^{\text{Nord}} = \alpha_2/2$.

Since we are interested in the relative orbital motion of the binary's components, we have to express eq. (5)-eq. (7) in terms of relative quantities³. From eq. (3)-eq. (4) it turns out,

$$\mathbf{v}_A^0 \cdot \mathbf{v}_B^0 = w^2 + \frac{\Delta m}{M} (\mathbf{v} \cdot \mathbf{w}) - \frac{m_A m_B}{M^2} v^2, \quad (8)$$

$$(\mathbf{v}_A^0 \cdot \hat{\mathbf{r}}) (\mathbf{v}_B^0 \cdot \hat{\mathbf{r}}) = w_r^2 + \frac{\Delta m}{M} w_r v_r - \frac{m_A m_B}{M^2} v_r^2, \quad (9)$$

where $v_r \doteq \mathbf{v} \cdot \hat{\mathbf{r}}$, $w_r \doteq \mathbf{w} \cdot \hat{\mathbf{r}}$, $\Delta m \doteq m_A - m_B$. Thus, eq. (5)-eq. (6) become

$$\mathcal{L}_{\alpha_1} = -\frac{\alpha_1 GM}{2c^2 r} \left[w^2 + \frac{\Delta m}{M} (\mathbf{v} \cdot \mathbf{w}) - \frac{m_A m_B}{M^2} v^2 \right], \quad (10)$$

$$\mathcal{L}_{\alpha_2} = -\frac{\alpha_2}{\alpha_1} \mathcal{L}_{\alpha_1} + \tilde{\mathcal{L}}_{\alpha_2}, \quad (11)$$

with

$$\tilde{\mathcal{L}}_{\alpha_2} = -\frac{\alpha_2 GM}{2c^2 r} \left(w_r^2 + \frac{\Delta m}{M} w_r v_r - \frac{m_A m_B}{M^2} v_r^2 \right). \quad (12)$$

²It is the ratio of the Lagrangian to the reduced mass $\mu \doteq m_A m_B / M$ of the binary system.

³The motion of the Sun with respect to the Solar System Barycenter (SSB) has been recently analyzed in [38].

By recalling that a general velocity-dependent perturbative Lagrangian $\mathcal{L}_{\text{pert}}$ yields a corresponding perturbative Hamiltonian [39–41]

$$\mathcal{H}_{\text{pert}} = -\mathcal{L}_{\text{pert}} - \frac{1}{2} \left(\frac{\partial \mathcal{L}_{\text{pert}}}{\partial \mathbf{v}} \right)^2, \quad (13)$$

the following PFE reduced Hamiltonians can be obtained, to order $\mathcal{O}(G/c^2)$, from eq. (10)-eq. (12)

$$\mathcal{H}_{\alpha_1} = \frac{\alpha_1 GM}{2c^2 r} \left[w^2 + \frac{\Delta m}{M} (\mathbf{v} \cdot \mathbf{w}) - \frac{m_A m_B}{M^2} v^2 \right], \quad (14)$$

$$\mathcal{H}_{\alpha_2} = -\frac{\alpha_2}{\alpha_1} \mathcal{H}_{\alpha_1} + \tilde{\mathcal{H}}_{\alpha_2}, \quad (15)$$

with

$$\tilde{\mathcal{H}}_{\alpha_2} = \frac{\alpha_2 GM}{2c^2 r} \left(w_r^2 + \frac{\Delta m}{M} v_r w_r - \frac{m_A m_B}{M^2} v_r^2 \right). \quad (16)$$

Perturbing accelerations can be obtained from eq. (14)-eq. (16) as

$$\dot{\mathbf{p}} = -\frac{\partial \mathcal{H}}{\partial \mathbf{r}} \quad (17)$$

by noting that

$$\mathbf{p}_{\alpha_1} \doteq \frac{\partial \mathcal{L}_{\alpha_1}}{\partial \mathbf{v}} = -\frac{\alpha_1 GM}{2c^2 r} \left(\frac{\Delta m}{M} \mathbf{w} - 2 \frac{m_A m_B}{M^2} \mathbf{v} \right), \quad (18)$$

$$\tilde{\mathbf{p}}_{\alpha_2} \doteq \frac{\partial \tilde{\mathcal{L}}_{\alpha_2}}{\partial \mathbf{v}} = -\frac{\alpha_2 GM}{2c^2 r} \left(\frac{\Delta m}{M} w_r - 2 \frac{m_A m_B}{M^2} v_r \right) \hat{\mathbf{r}}. \quad (19)$$

3 Averaged orbital perturbations

An effective method to analytically calculate the orbital effects induced by a generic small correction $\mathcal{H}_{\text{pert}}$ to the Newtonian potential $U_N = -GM/r$ consists of evaluating $\mathcal{H}_{\text{pert}}$ over the unperturbed Keplerian ellipse, assumed as reference trajectory, and averaging it over one orbital period P_b of the test particle. Then, the Lagrange perturbation equations [41–43] allow to straightforwardly calculate to first order the long-term rates of change of the orbital elements by means of partial derivatives of $\langle \mathcal{H}_{\text{pert}} \rangle$ with respect to them. In principle, it would be possible to adopt a different reference

trajectory as unperturbed orbit including also general relativity at the 1PN level and use the so-called post Newtonian Lagrange planetary equations [44, 45]. Nonetheless, in the specific case of eq. (14)-eq. (16), in addition to the first order precessions of order $\mathcal{O}(c^{-2})$ coming from the use of the Newtonian reference trajectory to be computed below, other “mixed” 1PN-PF precessions of higher order would arise specifying the influence of PFE on the 1PN post-Keplerian orbital motion assumed as unperturbed. From the point of view of constraining α_1, α_2 from observations, they are practically negligible since their magnitude is quite smaller than the first order terms.

Before performing the calculation, a consideration about the orbital elements employed in it is in order. Strictly speaking, since the perturbing Hamiltonians of eq. (14)-eq. (16) depend also upon the velocity \mathbf{v} , inserting them into the usual Lagrange variation equations yields nonosculating orbital elements called contact elements [46], which are not tangent to the perturbed trajectory [39, 47]. If certain general conditions on the periodicity of motion are satisfied [41], the averaging procedure reduces the difference between the contact and the osculating elements in such a way that residual differences occur only to higher order. See [48] for a preliminary discussion of this issue in the present context. As it will be discussed in Section 4, it is just what occurs in the present case.

The semimajor axis a , which is dimensionally a length characterizing the size of the orbit, varies according to the Lagrange equation [41, 42]

$$\left\langle \frac{da}{dt} \right\rangle = -\frac{2}{n_b a} \frac{\partial \langle \mathcal{H}_{\text{pert}} \rangle}{\partial \mathcal{M}_0}. \quad (20)$$

In it, $n_b \doteq \sqrt{GM/a^3}$ is the Keplerian mean motion in terms of which the orbital period is expressed as $P_b = 2\pi/n_b$; its dimensions are those of a frequency. The angle \mathcal{M}_0 is the mean anomaly at the epoch t_0 [41].

The Lagrange equation for the eccentricity e , which is a dimensionless numerical parameter determining the shape of the ellipse in such a way that⁴ $0 \leq e < 1$, is [41, 42]

$$\left\langle \frac{de}{dt} \right\rangle = \frac{1}{n_b a^2} \left(\frac{1 - e^2}{e} \right) \left[\frac{1}{\sqrt{1 - e^2}} \frac{\partial \langle \mathcal{H}_{\text{pert}} \rangle}{\partial \omega} - \frac{\partial \langle \mathcal{H}_{\text{pert}} \rangle}{\partial \mathcal{M}_0} \right]. \quad (21)$$

In it, the argument of pericenter ω is an angle in the orbital plane counted from the line of the nodes (see below) to the point of closest approach. Although not yet explicitly determined for Solar System’s planets [49], the

⁴A circular orbit corresponds to $e = 0$.

rate of change of e is actually measured in some binary pulsar systems [37, 50, 51].

The inclination I of the orbital plane to the reference $\{x, y\}$ plane⁵ Its rate of change has not yet been explicitly determined by the astronomers for planets of the Solar System [49]. On the other hand, its precession is one of the observable quantities in binary pulsar studies through its connection with the projected semimajor axis $x_p \doteq a_p \sin I/c$, where a_p is the barycentric semimajor axis of the pulsar. Indeed, its rate of change \dot{x}_p is often accessible to observation in several binaries [37, 50, 51]. The Lagrange equation for I is [41, 42]

$$\left\langle \frac{dI}{dt} \right\rangle = \frac{1}{n_b a^2 \sqrt{1-e^2} \sin I} \left[\frac{\partial \langle \mathcal{H}_{\text{pert}} \rangle}{\partial \Omega} - \cos I \frac{\partial \langle \mathcal{H}_{\text{pert}} \rangle}{\partial \omega} \right]. \quad (22)$$

In it, the longitude of the ascending node Ω is an angle in the $\{x, y\}$ reference plane counted from the x reference direction to the line of the nodes which, in turn, is the intersection of the orbital plane with the $\{x, y\}$ plane itself.

The node is one of the orbital parameters used by the astronomers [49] to constrain putative non-standard dynamical effects in the Solar System. Sometimes, it is measurable also in specific binary pulsars [52–54]. The long-term precession of Ω is computed from the Lagrange perturbation equation [41, 42]

$$\left\langle \frac{d\Omega}{dt} \right\rangle = -\frac{1}{n_b a^2 \sqrt{1-e^2} \sin I} \frac{\partial \langle \mathcal{H}_{\text{pert}} \rangle}{\partial I}. \quad (23)$$

The longitude of pericenter $\varpi \doteq \Omega + \omega$, which is a “broken” angle, is another parameter usually adopted in both Solar System and binary pulsars studies to put limits on putative exotic forces [49]. Its Lagrange perturbation equation is [41, 42]

$$\left\langle \frac{d\varpi}{dt} \right\rangle = -\frac{1}{n_b a^2} \left[\left(\frac{\sqrt{1-e^2}}{e} \right) \frac{\partial \langle \mathcal{H}_{\text{pert}} \rangle}{\partial e} + \frac{\tan\left(\frac{I}{2}\right)}{\sqrt{1-e^2}} \frac{\partial \langle \mathcal{H}_{\text{pert}} \rangle}{\partial I} \right]. \quad (24)$$

In principle, also the mean anomaly $\mathcal{M} = \mathcal{M}_0 + n_b(t - t_0)$ [41] should be considered, but it will not be treated here since its precession is neither determined in Solar System analyses of planetary motions nor in binary pulsars. Indeed, its accuracy is necessarily limited by the uncertainty in the

⁵It is the plane of the sky in the case of a celestial binary system such as, e.g., a binary pulsar, while it is customarily the Earth’s mean equator at the epoch J2000.0 if the planets of our Sun are considered.

gravitational parameter GM entering n_b , making the use of \mathcal{M} usually less competitive than the other orbital elements.

Other analytical calculations of the orbital effects of non-vanishing α_1, α_2 , made with different computational strategies and based on various levels of approximation, can be found in, e.g., [36, 37, 48, 55, 56].

Our analytical expressions for the α_1, α_2 long-term precessions are displayed in Appendix A and Appendix B. As fast variable of integration in averaging eq. (14)-eq. (16), it turned out computationally more convenient to adopt the eccentric anomaly E . Nonetheless, as a further check, we repeated the calculation with the true anomaly f as well: the same results were re-obtained.

4 Confrontation with the observations

The analytical results of Appendix A and Appendix B were successfully confirmed by numerically integrating the equations of motion of a test particle including the PF accelerations coming from eq. (17) with eq. (14)-eq. (16) and eq. (18)-eq. (19) over a given time interval, and plotting the temporal evolution of the numerically computed orbital elements with the standard formulas of the osculating Keplerian elements. In Figure 1 and Figure 2 the plots for Mercury over one century, obtained for $\alpha_1 = \alpha_2 = 1$ just for illustrative purposes and with eq. (43) for \boldsymbol{w} , are displayed. They yield the same centennial rates obtainable from the analytical formulas of Appendix A and Appendix B for the contact elements, computed for the same values of $\alpha_1, \alpha_2, \boldsymbol{w}$ used in the numerical integration. This shows that, to the approximation level used in the calculation, the contact elements are equal to the osculating elements.

Thus, confident in our results of Appendix A-Appendix B, we are going to apply them to effectively constrain both α_1 and α_2 from latest determinations of planetary orbital motions [49]. In Section 4.1 we critically review the bounds existing in literature.

4.1 Discussion of the constraints existing in literature

As a general rule pertaining the bounds on the strong-field equivalent $\hat{\alpha}_1, \hat{\alpha}_2$ with compact object, Shao and Wex [37] interestingly remark that their general validity may be questioned by a potential compactness-dependence (or mass-dependence) of $\hat{\alpha}_1, \hat{\alpha}_2$ because of certain peculiar phenomena, such as spontaneous scalarization [58], which may take place. Thus, Shao and Wex [37] warn that it is always recommendable to specify the binary system

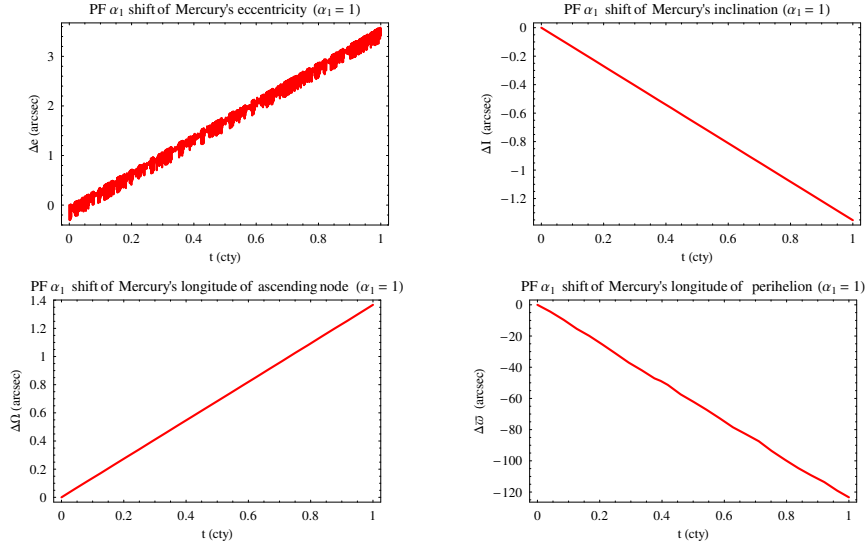


Figure 1: Numerically integrated temporal evolutions of the total PF α_1 -induced shifts (in arcsec) of the eccentricity e , the inclination I , the longitude of the ascending node Ω and the longitude of perihelion ϖ of Mercury over one century. They were obtained by numerically integrating the planet's equations of motion in cartesian coordinates with and without the perturbative accelerations arising from eq. (14) by using the same initial conditions retrieved from the NASA JPL HORIZONS System (<http://ssd.jpl.nasa.gov/?horizons>). For illustrative purposes the value $\alpha_1 = 1$ was chosen. The figures in eq. (43), taken from [57], were adopted for \mathbf{w} . The resulting centennial rates are in agreement with the sum of those computed from the analytical formulas in Appendix A.

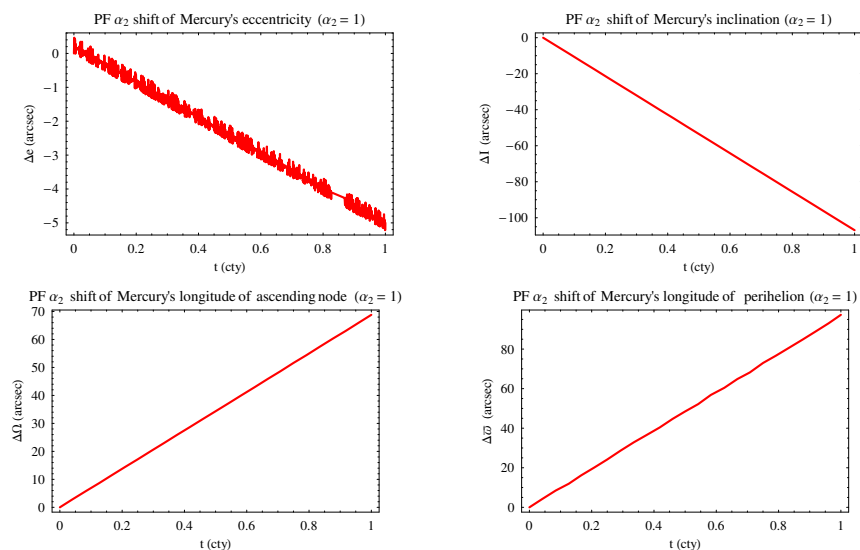


Figure 2: Numerically integrated temporal evolutions of the total PF α_2 -induced shifts (in arcsec) of the eccentricity e , the inclination I , the longitude of the ascending node Ω and the longitude of perihelion ϖ of Mercury over one century. They were obtained by numerically integrating the planet’s equations of motion in cartesian coordinates with and without the perturbative accelerations arising from eq. (15)-eq. (16) by using the same initial conditions retrieved from the NASA JPL HORIZONS System (<http://ssd.jpl.nasa.gov/?horizons>). For illustrative purposes the value $\alpha_2 = 1$ was chosen. The figures in eq. (43), taken from [57], were adopted for \mathbf{w} . The resulting centennial rates are in agreement with the sum of those computed from the analytical formulas in Appendix B.

used to infer given constraints on $\hat{\alpha}_1, \hat{\alpha}_2$. Another limitation of the strong-field tests is their probabilistic nature since the orbital configurations of the binaries used are not always completely known: indeed, the longitudes of the ascending nodes Ω are often unknown, and also the inclinations I may be sometimes determined modulo the ambiguity of $I \rightarrow 180^\circ - I$.

4.1.1 α_1

Earlier constraints on α_1 were obtained from Solar System planetary motions [55,59] and Lunar Laser Ranging [60]; the most accurate bounds [59,60] were at $\approx 2 \times 10^{-4}$ level.

Strong-field tests were reported by using compact objects such as neutron stars and white dwarfs [36, 61]. They were able to constrain $\hat{\alpha}_1$, which, in principle, may differ from the weak-field value α_1 because of possible contributions from strong-field effects, down to $5.0 - 1.2 \times 10^{-4}$. Latest bounds on $\hat{\alpha}_1$ were obtained by Shao and Wex [37] from the neutron star-white dwarf binary PSR J1738+0333 [62] yielding $|\hat{\alpha}_1| = -0.4_{-3.1}^{+3.7} \times 10^{-5}$.

4.1.2 α_2

Concerning α_2 , Nordtvedt [35] inferred an upper bound of the order of 10^{-7} from the close alignment of the Sun's angular momentum with the total angular momentum of the Solar System. Nonetheless, as remarked by Shao and Wex [37], such a result strongly depends on the assumption that the two angular momenta were aligned just after the formation of the Solar System about 5 Gyr ago. If compared to the well known planetary orbital motions and the dynamical forces determining them, the hypothesis on which the analysis by Nordtvedt [35] is based is relatively more speculative and less testable. Another potential issue of the Nordtvedt reasoning [35] may be the following one.

The orientation of the Solar System's invariable plane [63] is fixed by the values of the celestial coordinates of its north pole: the right ascension α (RA) and the declination δ (DEC). At epoch J2000.0, they are [64]

$$\alpha_{\text{inv}} = 273.85^\circ, \delta_{\text{inv}} = 66.99^\circ; \quad (25)$$

thus, its normal unit vector $\hat{\mathbf{L}}$ is

$$\hat{L}_x = \cos \delta_{\text{inv}} \cos \alpha_{\text{inv}} = 0.03, \quad (26)$$

$$\hat{L}_y = \cos \delta_{\text{inv}} \sin \alpha_{\text{inv}} = -0.39, \quad (27)$$

$$\hat{L}_z = \sin \delta_{\text{inv}} = 0.92. \quad (28)$$

The north pole of rotation of the Sun at J2000.0 is characterized by [64]

$$\alpha_{\odot} = 286.13^{\circ}, \delta_{\odot} = 63.87^{\circ}, \quad (29)$$

so that the Sun's spin axis $\hat{\mathbf{S}}^{\odot}$ is

$$\hat{S}_x^{\odot} = 0.122, \quad (30)$$

$$\hat{S}_y^{\odot} = -0.423, \quad (31)$$

$$\hat{S}_z^{\odot} = 0.897. \quad (32)$$

Thus, the angle between the Sun's spin axis $\hat{\mathbf{S}}$ and the Solar System's total angular momentum \mathbf{L} is

$$\theta_{LS} = 5.97^{\circ}. \quad (33)$$

While the orientation of the invariable plane is nowadays quite accurate, being at $\approx 0.1 - 0.3 \text{ mas cty}^{-1}$ level [63], it is not so for the Sun's spin axis. Indeed, its determination is usually made in terms of the Carrington elements [65,66] i , which is the angle from the Sun's equator to the ecliptic, and the longitude of the node Ω of the Sun's equator with respect to the Vernal equinox Υ along the ecliptic, by means of

$$\hat{s}_x^{\odot} = \sin i \sin \Omega, \quad (34)$$

$$\hat{s}_y^{\odot} = -\sin i \cos \Omega, \quad (35)$$

$$\hat{s}_z^{\odot} = \cos i. \quad (36)$$

Beck and Giles [67] recently measured them from time-distance helioseismology analysis of Dopplergrams from the Michelson Doppler Imager (MDI)

instrument on board the SOlar and Heliospheric Observatory (SOHO) spacecraft; the data span was $\Delta t' = 5$ yr, from May 1996 through July 2001. The resulting values are⁶

$$i = 7.155^\circ \pm 0.002^\circ, \quad (37)$$

$$\Omega = 73.5^\circ \pm 1^\circ. \quad (38)$$

Maybe a better accuracy could be reached in a near future with a dynamical measurement from planetary orbital motions by exploiting the general relativistic Lense-Thirring effect [68]. The figures of eq. (37)-eq. (38) imply an ability to observationally constrain putative rates of change of θ_{LS} ($i, \Omega, \alpha_{\text{inv}}, \delta_{\text{inv}}$) with a necessarily limited accuracy; it can approximately be evaluated as

$$\sigma_{\dot{\theta}_{LS}} \approx \frac{\sqrt{\left(\frac{\partial\theta_{LS}}{\partial i}\right)^2 \sigma_i^2 + \left(\frac{\partial\theta_{LS}}{\partial\Omega}\right)^2 \sigma_\Omega^2}}{\Delta t'} = 7.73 \times 10^2 \text{ arcsec yr}^{-1}. \quad (39)$$

It is an important limiting factor when hypothesized secular rates $\dot{\theta}_{LS}$ are used to constrain parameters entering the models proposed to explain θ_{LS} .

It is just the case as far as α_2 is concerned. Indeed, Nordtvedt [35] noticed that one of the dynamical consequences of the first term in eq. (16) is a torque τ_{α_2} causing a precession of the Sun's spin axis about \mathbf{w} at a rate Ξ_{α_2} proportional to α_2 . Competing classical torques due to the planets of the Solar System induce an extremely low overall precession of the Sun's spin axis characterized by a rate [35] $\Xi_{\text{class}} \approx 10^{-10} \text{ yr}^{-1}$. Under certain simplifying assumptions, Nordtvedt [35] obtained

$$\sin\left(\frac{\theta_{LS}}{2}\right) = \left(\frac{\Xi_{\alpha_2}}{\Xi_{\text{class}}}\right) \sin\left(\frac{\Xi_{\text{class}} t}{2}\right). \quad (40)$$

By assuming that the Sun's equator and the invariable plane were aligned at the birth of the Solar System 5 Gyr ago, and that the present-day value of eq. (33) is due to the steady action of the aforementioned torques throughout the life of the Solar System in such a way that $\Xi_{\text{class}} \Delta T / 2 \ll 1$, $\Delta T = 5$ Gyr, eq. (40) reduces to

$$\theta_{LS} \approx \Xi_{\alpha_2} \Delta T. \quad (41)$$

⁶After rotating eq. (34)-eq. (36), calculated with eq. (37)-eq. (38), from the ecliptic to the Earth's equator, eq. (30)-eq. (32) are obtained.

In other words, the PF α_2 -induced spin precession would cause a secular rate of change $\dot{\theta}_{LS}$ whose magnitude is approximately equal to Ξ_{α_2} . By posing $\Delta T = 5$ Gyr, Nordtvedt [35] inferred an upper limit of α_2 as little as $\approx 10^{-7}$ from a hypothesized precession

$$\dot{\theta}_{LS} = \frac{5.97^\circ}{5 \text{ Gyr}} = 4 \times 10^{-6} \text{ arcsec yr}^{-1}. \quad (42)$$

In fact, apart from the more or less speculative assumptions about a dynamical evolution spanning 5 Gyr, the observational uncertainty in actually measuring such a kind of time derivative of θ_{LS} should be considered in deriving realistic constraints on α_2 . As we have seen, the errors in determining the Carrington elements of the Sun's spin axis yield an uncertainty in observationally constraining $\dot{\theta}_{LS}$ which may be about 8 orders of magnitude larger than eq. (42).

For previous tests involving also other phenomena such as, e.g., Earth tides, see [3, 69].

Moving to the strong-field regime, Shao and Wex [37] reported $|\hat{\alpha}_2| \leq 1.8 \times 10^{-4}$ from the rate of change of the projected semimajor axis of the two pulsar-white dwarf binaries PSR J1012+5307 [70] and PSR J1738+0333 [62]. Earlier limits ($-0.3 < \hat{\alpha}_2 < 0.2$) were inferred by Wex and Kramer [56] by using the double pulsar PSR J0737-3039A/B [71] made of two neutron stars. As remarked by Shao and Wex [37] themselves, a potential drawback of their latest constraint on $\hat{\alpha}_2$ is that it was obtained by combining data from two systems whose neutron stars have different masses. Moreover, a straightforward comparison with the previous test by Wex and Kramer [56] is, in principle, problematic because the latter probed the interaction between two strongly self-gravitating objects, while the systems used by Shao and Wex [37] contain white dwarfs.

4.2 Bounds from recent Solar System planetary data

According to Table 1, the present-day accuracy in constraining possible extra-precessions of the nodes and perihelia with respect to standard Newtonian/Einsteinian effects has reached the $\approx 1 - 0.5$ milliarcseconds per century (mas cty^{-1}) level for the inner planets of the Solar System and for Saturn. This fact, in conjunction with the theoretical predictions of Appendix A and Appendix B, allows to infer tight constraints on both α_1 and α_2 .

We note that Fienga et al. [49] neither explicitly modelled PFE nor simultaneously estimated α_1, α_2 along with the other solved-for parameters

Table 1: Supplementary precessions $\Delta\dot{\Omega}$, $\Delta\dot{\varpi}$ of the longitudes of the node and of the perihelion for some planets of the Solar System estimated by Fienga et al. [49] with the INPOP10a ephemerides. Actually, more recent versions of the INPOP ephemerides, named INPOP10e [72] and INPOP13a [38], have been recently produced; no supplementary orbital precessions have yet been released for them. The reference $\{x, y\}$ plane is the mean Earth’s equator at J2000.0. The units are milliarcseconds per century (mas cty^{-1}). Fienga et al. [49] did not model PFE by keeping the values of the PPN parameters β, γ fixed to their general relativistic values. Thus, their supplementary precessions $\Delta\dot{\Omega}$, $\Delta\dot{\varpi}$ effectively account for any kind of departures from standard dynamics in a model-independent way.

	$\Delta\dot{\Omega}$ (mas cty^{-1})	$\Delta\dot{\varpi}$ (mas cty^{-1})
Mercury	1.4 ± 1.8	0.4 ± 0.6
Venus	0.2 ± 1.5	0.2 ± 1.5
Earth	0.0 ± 0.9	-0.2 ± 0.9
Mars	-0.05 ± 0.13	-0.04 ± 0.15
Saturn	-0.1 ± 0.4	0.15 ± 0.65

of their analysis. Thus, it may be speculated that the bounds obtained here by straightforwardly comparing our analytical predictions with the extra-precessions of Table 1 are too optimistic since, e.g., a hypothetically existing PFE signal may have been partially removed from the residuals, being somewhat absorbed into the values of the estimated parameters such as, say, the planetary state vectors. In other words, there may be still room for larger values of α_1, α_2 than those inferred by us. Actually, we are not convinced that such an objection can invalidate our findings, although fitting suitably modified dynamical models to the same planetary observations and estimating α_1, α_2 simultaneously with, e.g., the other PPN parameters would certainly be a useful complementary approach which could also broaden the range of applicability of the resulting constraints (see below). On the one hand, one could always argue that, even by explicitly solving for PFE, the resulting constraints on α_1, α_2 may still be impacted by any other sort of unmodelled/mismodelled forces, both standard and exotic. Indeed, a selection of the dynamical effects to be modelled and of the parameters entering them which can be practically estimated is always made in real data reduction. Thus, the effect of any sort of “Russell teapots” may well creep

into the the solved-for values of α_1, α_2 estimated in a full covariance analysis. On the other hand, the existing literature shows that, actually, our approach has been often adopted in other studies using planetary data to constrain non-standard effects (Dark Matter [73, 74], MOND [75], general departures from inverse-square law [76], etc.). Nordtvedt himself [35] based his analysis on already existing observations previously reduced by the astronomers who did not model PFE at all and assumed a-priori the validity of general relativity; his constraint on α_2 [35] does not come from a fit of dynamical models including PFE. Moreover, we believe that the validity of our approach was indirectly confirmed, at least for certain hypothetical extra-forces, in independent analyses by some astronomers who explicitly dealt with certain anomalous effects of interest. Indeed, in the case of, e.g., the Pioneer anomaly [77, 78], we concluded [79] that it could not be caused by an exotic gravitational mechanism just by comparing the predicted planetary perihelion precessions due to a uniform acceleration radially directed towards the Sun with the limits of the anomalous planetary perihelion precessions obtained by some astronomers without explicitly modeling such a putative acceleration. In subsequent researches, either ad-hoc modified dynamical planetary theories were fitted by some astronomers to data records of increasing length and quality getting quite negative results for values of the anomalous radial acceleration as large as the Pioneer one [80–83], or they explicitly modeled and solved for a constant, radial acceleration inferring admissible upper bounds [84] not weaker than those obtained by us [85]. On the contrary, to our knowledge, there are no published papers in which real planetary data were processed to constrain some exotic accelerations by explicitly estimating them which show a substantial discrepancy with the results obtained with our approach. A partial exception may be represented by the interesting work by Hees et al. [86] in which certain modified models of gravity were fitted to simulated observations and some dedicated parameters were determined. Nonetheless, its validity could well be limited just to the specific effect investigated and to the data simulation procedure adopted. Last but not least, it would be difficult to understand how Le Verrier [87] successfully measured the anomalous perihelion precession of Mercury by processing its observations with purely Newtonian models. The completely unmodelled general relativistic signature was not removed from the residuals, thus allowing Einstein [88] to solve the puzzle of the Mercury’s anomalous motion just by comparing his theoretical precession with the existing observational determination. Finally, we remark that our constraints on α_1, α_2 should not be considered as too optimistic also because we assumed that the whole range of variation of the extra-precessions in Table 1

is entirely due to PFE. On the other hand, it must also be admitted that such a choice somewhat restricts the range of applicability of our results. Indeed, by using observationally-determined quantities such as the supplementary perihelion precessions of Table 1 obtained by keeping the other PPN parameters fixed to their general relativistic values implies that the hypothetical PFE theory constrained by us deviates from general relativity in at most⁷ α_1, α_2 .

As far as \mathbf{w} is concerned, a natural choice for the preferred frame, common to the literature on preferred-frame effects [35–37, 48, 59, 69], is the Cosmic Microwave Background (CMB). With such a choice one is quite plausibly assuming that the preferred frame is determined by the global matter distribution of the Universe, with the extra-components of the gravitational interaction ranging over scales at least comparable to the Hubble radius. Latest results from the Wilkinson Microwave Anisotropy Probe (WMAP) yield a peculiar velocity of the Solar System Barycenter (SSB) of [57]

$$w = 369.0 \pm 0.9 \text{ km s}^{-1}, l = 263.99^\circ \pm 0.14^\circ, b = 48.26^\circ \pm 0.03^\circ, \quad (43)$$

where l and b are the Galactic longitude and latitude, respectively. Thus, in Celestial coordinates, the components of the unit vector $\hat{\mathbf{w}}$ are

$$\hat{w}_x = -0.970, \quad (44)$$

$$\hat{w}_y = 0.207, \quad (45)$$

$$\hat{w}_z = -0.120. \quad (46)$$

By comparing the figures in Table 1 with the theoretical predictions of Appendix A and Appendix B, computed with eq. (44)-eq. (46), it is possible to infer upper bounds on α_1 and α_2 . It turns out that, in general, the nodes yield weaker constraints than the perihelia, especially as far as α_1 is concerned. Thus, in Table 2 only the bounds from the perihelia are displayed. The most stringent constraint on α_1 comes from the perihelion of Earth, amounting to $|\alpha_1| \lesssim 10^{-6}$. The perihelion of Mercury yields the tightest constraint for α_2 , which is of the order of $|\alpha_2| \lesssim 10^{-6}$ as well. In principle, the bounds of Table 2 may be biased by certain standard dynamical effects which were not modeled at all by Fienga et al. [49], such as

⁷From this point of view, some distinctive symbols such as, say, a tilde may have been adopted for the PFE parameters actually constrained in this paper in much the same way as a hat was put on their strong-field values. We did not so to avoid a too cumbersome notation.

Table 2: Constraints on α_1 and α_2 obtained from a straightforward comparison of the figures of Table 1 for the supplementary rates of the planetary perihelia with the theoretical predictions of Appendix A and Appendix B, calculated with eq. (43). The tightest bounds comes from the perihelion of Earth (α_1) and of Mercury (α_2).

	α_1	α_2
Mercury	$(-3 \pm 5) \times 10^{-6}$	$(4 \pm 6) \times 10^{-6}$
Venus	$(-0.1 \pm 1.1) \times 10^{-5}$	$(-0.7 \pm 5.7) \times 10^{-5}$
Earth	$(0.8 \pm 4) \times 10^{-6}$	$(-0.8 \pm 3.7) \times 10^{-5}$
Mars	$(-0.8 \pm 2.9) \times 10^{-5}$	$(0.4 \pm 1.5) \times 10^{-5}$
Saturn	$(-1.94 \pm 8.41) \times 10^{-4}$	$(1.95 \pm 8.5) \times 10^{-4}$

the general relativistic Lense-Thirring effect [89], thus impacting the supplementary rates $\Delta\dot{\varpi}$ of Table 1. The gravitomagnetic precession should not be neglected since its expected value (-2.0 mas cty^{-1}) is larger than the current uncertainty in the Mercury’s perihelion extra-rate (0.6 mas cty^{-1}); see [68] for a recent discussion of this aspect. Another standard effect which may a-priori impact the bounds in Table 2 through its lurking in Table 1 is the Newtonian perihelion precession due to the Sun’s quadrupole moment J_2 . Although its dynamical effect was fully modeled by Fienga et al. [49], a lingering uncertainty of [90] $\approx 10\%$ still affects J_2 in such a way that a resulting mismodelled perihelion precession certainly contributes to the figures in Table 1. The availability of more than one supplementary perihelion rate is a great advantage since it allows to set up a suitable linear combination involving the perihelia of the four inner planets able to separate, by construction, α_1 , α_2 from J_2 and the Lense-Thirring effect. This method has been used in a number of papers in the literature; it was proposed for the first time in [91, 92], as far as the Solar System planetary scenario is concerned. From the following linear system of four equations in the four unknowns $\alpha_1, \alpha_2, J_2, \mu_{\text{LT}}$

$$\Delta\dot{\varpi}^j = \alpha_1 \dot{\varpi}_{\alpha_1}^j + \alpha_2 \dot{\varpi}_{\alpha_2}^j + J_2 \dot{\varpi}_{J_2}^j + \mu_{\text{LT}} \dot{\varpi}_{\text{LT}}^j, \quad j = \text{Mercury} \dots \text{Mars}, \quad (47)$$

where the coefficients $\dot{\varpi}$ are the analytical expressions of the pericenter

precessions caused by the effects considered⁸, it is possible to obtain

$$\alpha_1 = (-1 \pm 6) \times 10^{-6}, \quad (48)$$

$$\alpha_2 = (-0.9 \pm 3.5) \times 10^{-5}, \quad (49)$$

$$J_2 = (1.4 \pm 4.1) \times 10^{-7}, \quad (50)$$

$$\mu_{LT} = 8 \pm 24. \quad (51)$$

By construction, the figures of eq. (48)-eq. (49) are not a-priori biased by any mismodeling in J_2 and by the Lense-Thirring effect, independently of their values. Incidentally, let us notice that, although not specifically designed for determining/constraining J_2, μ_{LT} , the system of eq. (47) yields figures for them (eq. (50) and eq. (51)) which are compatible with their expected values.

The constraints of Table 2 and of eq. (48)-eq. (49) will likely be further improved in the next few years. Indeed, our knowledge of the orbit of Mercury will be greatly enhanced when the entire data set of the MESSENGER spacecraft [94], which was inserted in orbit around Mercury in March 2011 for a year-long science phase extended until March 2013, will be processed. Another planned mission to Mercury is BepiColombo [95]: it will be launched in 2015 and should reach its target in 2022. One of its experiment is MORE [96]; it should further improve the determination of the orbit of Mercury [97]. For existing studies concerning, among other things, the opportunity of constraining also α_1 and α_2 with BepiColombo using different approaches, see [32, 33]. The covariance analysis in [32], based on a full cycle simulation of the BepiColombo radio science experiments, shows that α_1 and α_2 can be constrained within⁹ $\simeq 8 \times 10^{-6}$ and $\simeq 10^{-6}$, respectively. The “modified worst-case” error analysis in [33], which is a quite different approach with respect to that adopted in [32], predicts accuracies of the order of $\simeq 2.1 \times 10^{-5} - 8.6 \times 10^{-7}$ (α_1) and $2.9 \times 10^{-6} - 1.2 \times 10^{-6}$ (α_2) depending on the assumed mission duration ranging from 1 yr to 8 yr. Such constraints are not too far from those in Table 2 and in eq. (48)-eq. (49), especially as far as α_1 is concerned.

⁸General expressions for the J_2 and Lense-Thirring pericenter precessions can be found in [93]. The coefficient μ_{LT} is one in general relativity.

⁹They are realistic, non-formal uncertainties [32].

5 Summary and conclusions

The long-term, i.e. averaged over one orbital revolution, precessions of the orbital elements of the relative motion of the components of a binary system due to non-zero values of the PPN parameters α_1 and α_2 inducing preferred-frame effects were analytically worked out to first-order with the perturbative Lagrange planetary equations. We did not recur to a-priori simplifying assumptions on the preferred-frame velocity \boldsymbol{w} and on the binary's orbital geometry. The analytical expressions of the precessions were successfully tested with a numerical integration which yielded the same results. It was also numerically checked that, to the order of approximation used, the contact orbital elements used in the analytical calculation are actually tangent, i.e. osculating, to the perturbed trajectory.

We critically discussed the existing bounds on α_1, α_2 . We remarked that the $\mathcal{O}(10^{-7})$ constraint on α_2 inferred by Nordtvedt from a hypothesized secular precession of the angle between the Sun's equator and the invariable plane of the Solar System throughout its entire existence should be considered as optimistic. Indeed, it did not take into account the measurement limits in actually constraining such a precession from observations in view of the lingering uncertainties in the Carrington elements i and, especially, Ω which determine the orientation of the Sun's spin axis.

Deviating from the approach followed so far in literature, we used the supplementary node and perihelion secular precessions $\Delta\dot{\Omega}, \Delta\dot{\varpi}$ of some planets of the Solar System, recently determined by some astronomers from an analysis of a centennial data record in building the INPOP10a ephemerides, to preliminarily constrain both α_1 and α_2 . Indeed, such supplementary precessions, by construction, account for any unmodelled/mismodelled dynamical effects with respect to the standard Einstein-Newton gravity in the sense that the PPN parameters of the post-Newtonian forces modelled were kept fixed to their standard general relativistic values. After having noticed that the perihelia give tighter constraints than the nodes, we linearly combined the supplementary perihelion precessions $\Delta\dot{\varpi}$ of Mercury, Venus, Earth, Mars to simultaneously solve for α_1, α_2 , and for the Sun's Lense-Thirring effect and oblateness J_2 as well. Indeed, they were unmodelled/mismodelled in the INPOP10a-based analysis and represent competing effects for the α_1, α_2 -induced precessions we are interested in. We obtained $\alpha_1 = (-1 \pm 6) \times 10^{-6}, \alpha_2 = (-0.9 \pm 3.5) \times 10^{-5}$. Our results, which retain a general validity for all the weak-field scenarios departing from general relativity just as far as PFE are concerned, are based on well tested dynamical effects pertaining known Solar System's objects, and do not rely

upon speculative assumptions about hypothesized phenomena for which no data actually exist. On the other hand, we inferred them by assuming that the ranges $\Delta\dot{\varpi}$ are entirely due to α_1, α_2 themselves; such a choice may somewhat limit the range of applicability of our results to just those PFE theories deviating from general relativity in at most α_1, α_2 themselves. As a complementary approach which, in principle, could be followed in dedicated full covariance analyses, the preferred-frame effects should be explicitly included in purposely modified dynamical models which should be fitted to the planetary data set, and α_1, α_2 should be simultaneously estimated along with the other PPN parameters. Nonetheless, its practical implementation is not at all trivial. It is worthwhile noticing that we did not limit ourselves just to the node and the pericenter, having computed the long-term rates of change also for the other Keplerian orbital elements exhibiting peculiar signatures with respect to other potentially competing dynamical effects. They could turn out useful in future if and when the astronomers will determine the ranges for their supplementary rates as well. Analogous considerations hold also for other astronomical systems.

Future improvements in the orbit determination of Mercury are expected in the near and mid future from MESSENGER and BepiColombo missions; they should allow to get tighter constraints on α_1, α_2 . In this respect, it is remarkable that the constraints expected from BepiColombo for both α_1 and α_2 in independent analyses are close to those inferred by us in this paper, especially as far as α_1 is concerned.

Appendices

A The α_1 precessions

The orbital precessions induced by eq. (14) can be conveniently computed by considering separately each of the three terms entering eq. (14). The following analytical expressions are exact in the sense that no a priori assumptions on the spatial orientation of \boldsymbol{w} were assumed. Moreover, the limits of small eccentricity and inclination were not assumed as well. It is worthwhile noticing that the mean anomaly at the epoch \mathcal{M}_0 does not enter the following averages of the perturbing Hamiltonians. Thus, according to eq. (20)-eq. (21), the semimajor axis a remains unaffected, while the eccentricity e may change only if the averaged Hamiltonians depend on the argument of pericenter ω .

A.1 The v^2 term

The average of the term proportional to the square of the two-body relative velocity in eq. (14) is

$$\langle \mathcal{H}_{\alpha_1}^{v^2} \rangle = \frac{\alpha_1 G n_b^2 m_A m_B a}{2c^2 M} \left(1 - \frac{2}{\sqrt{1-e^2}} \right). \quad (\text{A.1})$$

Thus, the long-term precessions caused by it are all zero, apart from the longitude of the pericenter. Its rate of change is

$$\left\langle \frac{d\varpi}{dt} \right\rangle = \frac{\alpha_1 G m_A m_B n_b}{c^2 a (1-e^2) M}. \quad (\text{A.2})$$

A.2 The w^2 term

All the precessions due to the term proportional to w^2 in eq. (14) vanish. Indeed, its average is

$$\langle \mathcal{H}_{\alpha_1}^{w^2} \rangle = \frac{\alpha_1 G w^2 M}{2ac^2}. \quad (\text{A.3})$$

A.3 The $(\mathbf{v} \cdot \mathbf{w})$ term

The average of the mixed term of eq. (14), proportional to Δm , is

$$\begin{aligned} \langle \mathcal{H}_{\alpha_1}^{\Delta m} \rangle = & \frac{\alpha_1 w G n_b \Delta m \left(-1 + e^2 + \sqrt{1-e^2} \right)}{2c^2 e \sqrt{1-e^2}} [\hat{w}_z \sin I \cos \omega + \\ & + \cos I \cos \omega (\hat{w}_y \cos \Omega - \hat{w}_x \sin \Omega) - \sin \omega (\hat{w}_x \cos \Omega + \hat{w}_y \sin \Omega)]. \end{aligned} \quad (\text{A.4})$$

It yields non-vanishing long-term variations for all the orbital elements, apart from a . They are

$$\begin{aligned} \left\langle \frac{de}{dt} \right\rangle &= -\frac{\alpha_1 w G \Delta m \left(-1 + e^2 + \sqrt{1 - e^2} \right)}{2c^2 a^2 e^2} \{ \cos \omega (\hat{w}_x \cos \Omega + \hat{w}_y \sin \Omega) + \\ &+ \sin \omega [\hat{w}_z \sin I + \cos I (\hat{w}_y \cos \Omega - \hat{w}_x \sin \Omega)] \}, \end{aligned} \quad (\text{A.5})$$

$$\begin{aligned} \left\langle \frac{dI}{dt} \right\rangle &= \frac{\alpha_1 w G \Delta m \left(-1 + e^2 + \sqrt{1 - e^2} \right) \sin \omega}{2c^2 a^2 e (1 - e^2)} [\hat{w}_z \cos I - \\ &- \sin I (\hat{w}_y \cos \Omega - \hat{w}_x \sin \Omega)], \end{aligned} \quad (\text{A.6})$$

$$\begin{aligned} \left\langle \frac{d\Omega}{dt} \right\rangle &= -\frac{\alpha_1 w G \Delta m \left(-1 + e^2 + \sqrt{1 - e^2} \right) \csc I \cos \omega}{2c^2 a^2 e (1 - e^2)} [\hat{w}_z \cos I - \\ &- \sin I (\hat{w}_y \cos \Omega - \hat{w}_x \sin \Omega)], \end{aligned} \quad (\text{A.7})$$

$$\begin{aligned} \left\langle \frac{d\varpi}{dt} \right\rangle &= \frac{\alpha_1 w G \Delta m}{2c^2 a^2 e} \left\{ \left(\frac{-1 + \sqrt{1 - e^2}}{e^2} \right) [\hat{w}_z \sin I \cos \omega + \right. \\ &+ \cos I \cos \omega (\hat{w}_y \cos \Omega - \hat{w}_x \sin \Omega) - \\ &- \sin \omega (\hat{w}_x \cos \Omega + \hat{w}_y \sin \Omega)] - \\ &- \left(\frac{-1 + e^2 + \sqrt{1 - e^2}}{1 - e^2} \right) \tan \left(\frac{I}{2} \right) \cos \omega [\hat{w}_z \cos I - \\ &- \sin I (\hat{w}_y \cos \Omega - \hat{w}_x \sin \Omega)] \}. \end{aligned} \quad (\text{A.8})$$

It turns out that the leading term in eq. (A.5) is of order $\mathcal{O}(e^0)$ in the eccentricity, while the next-to-leading order one is of order $\mathcal{O}(e^2)$. As far as I and Ω are concerned, their leading order terms are of order $\mathcal{O}(e)$, while

the first non-vanishing terms of higher order in e are of order $\mathcal{O}(e^3)$. The pericenter precession of eq. (A.8) has a term of order $\mathcal{O}(e^{-1})$, while the next ones are of order $\mathcal{O}(e)$ and $\mathcal{O}(e^3)$, respectively.

B The α_2 precessions

The orbital precessions due to α_2 are the same as of Appendix A rescaled by $-\alpha_2/\alpha_1$, and by those coming from eq. (16). Also in this case, analytical expressions exact in \boldsymbol{w}, e, I are obtained.

B.1 The v_r^2 term

The average of the term proportional to v_r^2 in eq. (16) is

$$\left\langle \tilde{\mathcal{H}}_{\alpha_2}^{v_r^2} \right\rangle = \frac{\alpha_2 G n_b^2 m_A m_B}{2c^2 M} \left(1 - \frac{1}{\sqrt{1-e^2}} \right). \quad (\text{B.9})$$

As a consequence, the long-term precessions induced by eq. (B.9) vanish, apart from ϖ . Its rate is

$$\left\langle \frac{d\varpi}{dt} \right\rangle = \frac{\alpha_2 G m_A m_B n_b}{2c^2 a (1-e^2) M}. \quad (\text{B.10})$$

B.2 The w_r^2 term

The average of the term proportional to w_r^2 in eq. (16) is

$$\begin{aligned} \left\langle \tilde{\mathcal{H}}_{\alpha_2}^{w_r^2} \right\rangle &= \frac{\alpha_2 w^2 n_b^2 a^2}{2c^2 e^2} \left\{ -\hat{w}_x^2 \sqrt{1-e^2} \cos^2 I \sin^2 \omega \sin^2 \Omega + \right. \\ &+ \hat{w}_x^2 \sqrt{1-e^2} \cos I \sin 2\omega \sin 2\Omega - 2\hat{w}_x \hat{w}_y \sqrt{1-e^2} \cos I \cos 2\Omega \sin 2\omega + \\ &+ \hat{w}_x \hat{w}_z \sqrt{1-e^2} \sin 2I \sin^2 \omega \sin \Omega + \hat{w}_x \hat{w}_y \sqrt{1-e^2} \cos^2 I \sin^2 \omega \sin 2\Omega + \\ &+ \hat{w}_x \hat{w}_y \sqrt{1-e^2} \sin^2 \omega \sin 2\Omega + \left[\hat{w}_x^2 \left(e^2 + \sqrt{1-e^2} - 1 \right) - \right. \\ &\left. - \hat{w}_y^2 \left(\sqrt{1-e^2} - 1 \right) \cos^2 I \right] \cos^2 \Omega \sin^2 \omega - \hat{w}_z^2 \sqrt{1-e^2} \sin^2 I \sin^2 \omega + \end{aligned}$$

$$\begin{aligned}
& + \hat{w}_y^2 \sqrt{1-e^2} \sin^2 \omega \sin^2 \Omega - \hat{w}_y \cos \Omega \sin^2 \omega \left[\hat{w}_z \left(\sqrt{1-e^2} - 1 \right) \sin 2I + \right. \\
& + \hat{w}_x \left(-2e^2 + \cos 2I + 3 \right) \sin \Omega \left. \right] + \sin^2 \omega \left(\hat{w}_z^2 \sin^2 I + \right. \\
& + \sin \Omega \left(\left(\hat{w}_y^2 \left(e^2 - 1 \right) + \hat{w}_x^2 \cos^2 I \right) \sin \Omega - \hat{w}_x \hat{w}_z \sin 2I \right) + \\
& + \hat{w}_y \cos I \sin 2\omega \left(2\hat{w}_x \cos 2\Omega + \hat{w}_y \sin 2\Omega \right) + \\
& + \cos^2 \omega \left(-2\hat{w}_x \hat{w}_z \cos I \sin I \sin \Omega e^2 + \left(\hat{w}_y^2 \left(e^2 + \sqrt{1-e^2} - 1 \right) \cos^2 I - \right. \right. \\
& - \hat{w}_x^2 \left(\sqrt{1-e^2} - 1 \right) \left. \left. \right) \cos^2 \Omega + \hat{w}_z^2 \left(e^2 + \sqrt{1-e^2} - 1 \right) \sin^2 I - \right. \\
& - \hat{w}_y^2 \sqrt{1-e^2} \sin^2 \Omega + \hat{w}_x^2 \sqrt{1-e^2} \cos^2 I \sin^2 \Omega + \\
& + \left(\hat{w}_y^2 + \left(e^2 - 1 \right) \hat{w}_x^2 \cos^2 I \right) \sin^2 \Omega + \hat{w}_x \hat{w}_z \left(1 - \sqrt{1-e^2} \right) \sin 2I \sin \Omega + \\
& + \hat{w}_y \hat{w}_z \cos \Omega \left(\left(e^2 + \sqrt{1-e^2} - 1 \right) \sin 2I - \right. \\
& - \hat{w}_x \left(2e^2 \cos^2 I + \sqrt{1-e^2} \left(\cos 2I + 3 \right) \right) \sin \Omega \left. \right) + \hat{w}_x \hat{w}_y \left(\cos^2 I + 1 \right) \sin 2\Omega + \\
& + 2 \sin 2\omega \left(\frac{1}{2} \cos I \left(\left(\hat{w}_x^2 \left(e^2 - 2 \right) - \hat{w}_y^2 \left(e^2 + 2\sqrt{1-e^2} \right) \right) \sin 2\Omega - \right. \right. \\
& \left. \left. - 2e^2 \hat{w}_x \hat{w}_y \cos 2\Omega \right) - \hat{w}_z \left(e^2 + 2\sqrt{1-e^2} - 2 \right) \sin I \left(\hat{w}_x \cos \Omega + \hat{w}_y \sin \Omega \right) \right) \left. \right\}.
\end{aligned} \tag{B.11}$$

The resulting non-vanishing long-term rates of change of the orbital elements are as follows.

$$\begin{aligned}
\left\langle \frac{de}{dt} \right\rangle &= \frac{\alpha_2 w^2 n_b \sqrt{1-e^2} \left(-2 + e^2 + 2\sqrt{1-e^2} \right)}{8c^2 e^3} \\
&\cdot \left\{ -8\hat{w}_z \sin I \cos 2\omega (\hat{w}_x \cos \Omega + \hat{w}_y \sin \Omega) + \right. \\
&+ 4 \cos I \cos 2\omega \left[-2\hat{w}_x \hat{w}_y \cos 2\Omega + (\hat{w}_x^2 - \hat{w}_y^2) \sin 2\Omega \right] + \\
&+ \sin 2\omega \left[(\hat{w}_x^2 - \hat{w}_y^2) (3 + \cos 2I) \cos 2\Omega + \right. \\
&+ 2 \sin^2 I (\hat{w}_x^2 + \hat{w}_y^2 - 2\hat{w}_z^2) - 4\hat{w}_z \sin 2I (\hat{w}_y \cos \Omega - \hat{w}_x \sin \Omega) + \\
&\left. + 2\hat{w}_x \hat{w}_y (3 + \cos 2I) \sin 2\Omega \right\}, \tag{B.12}
\end{aligned}$$

$$\begin{aligned}
\left\langle \frac{dI}{dt} \right\rangle &= \frac{\alpha_2 w^2 n_b}{2c^2 e^2 \sqrt{1-e^2}} \left[\hat{w}_z \cos I - \sin I (\hat{w}_y \cos \Omega - \hat{w}_x \sin \Omega) \right] \cdot \\
&\cdot \left\{ -2\sqrt{1-e^2} \hat{w}_x \cos \Omega \sin^2 \omega + \right. \\
&+ 2\sqrt{1-e^2} \hat{w}_y \cos I \cos \Omega \sin 2\omega - \\
&- 2\sqrt{1-e^2} \hat{w}_y \sin \Omega \sin^2 \omega + \\
&+ 2\sqrt{1-e^2} \cos^2 \omega (\hat{w}_x \cos \Omega + \hat{w}_y \sin \Omega) - \\
&- 2 \cos 2\omega (\hat{w}_x \cos \Omega + \hat{w}_y \sin \Omega) - \\
&- 2e^2 \sin^2 \omega (\hat{w}_x \cos \Omega + \hat{w}_y \sin \Omega) + \\
&\left. + 2\sqrt{1-e^2} \sin 2\omega [\hat{w}_z \sin I - \hat{w}_x \cos I \sin \Omega] + \right.
\end{aligned}$$

$$+ (-2 + e^2) \sin 2\omega [\hat{w}_z \sin I + \cos I (\hat{w}_y \cos \Omega - \hat{w}_x \sin \Omega)] \}, \quad (\text{B.13})$$

$$\begin{aligned} \left\langle \frac{d\Omega}{dt} \right\rangle &= -\frac{\alpha_2 w^2 n_b \csc I}{2c^2 e^2 \sqrt{1-e^2}} [\hat{w}_z \cos I - \sin I (\hat{w}_y \cos \Omega - \hat{w}_x \sin \Omega)] \cdot \\ &\cdot \left\{ \hat{w}_z \sin I \left[e^2 + \left(-2 + e^2 + 2\sqrt{1-e^2} \right) \cos 2\omega \right] + \right. \\ &+ \cos I \left[e^2 + \left(-2 + e^2 + 2\sqrt{1-e^2} \right) \cos 2\omega \right] (\hat{w}_y \cos \Omega - \hat{w}_x \sin \Omega) - \\ &\left. - \left(-2 + e^2 + 2\sqrt{1-e^2} \right) \sin 2\omega (\hat{w}_x \cos \Omega + \hat{w}_y \sin \Omega) \right\}, \quad (\text{B.14}) \end{aligned}$$

$$\begin{aligned} \left\langle \frac{d\varpi}{dt} \right\rangle &= \frac{\alpha_2 w^2 n_b}{8c^2 e^4} \cdot \\ &\cdot \left\{ \left(-2 + e^2 + 2\sqrt{1-e^2} \right) \cdot \right. \\ &\cdot [(\hat{w}_x^2 - \hat{w}_y^2) (3 + \cos 2I) \cos 2\Omega \cos 2\omega + \\ &+ 2(\hat{w}_x^2 + \hat{w}_y^2 - 2\hat{w}_z^2) \sin^2 I \cos 2\omega - \\ &- 4\hat{w}_z \sin 2I (\hat{w}_y \cos \Omega - \hat{w}_x \sin \Omega) \cos 2\omega + \\ &+ 2\hat{w}_x \hat{w}_y (3 + \cos 2I) \sin 2\Omega \cos 2\omega + \\ &+ 8\hat{w}_z \sin I (\hat{w}_x \cos \Omega + \hat{w}_y \sin \Omega) \sin 2\omega + \\ &+ 8\hat{w}_x \hat{w}_y \cos I \cos 2\Omega \sin 2\omega - \\ &\left. - 4(\hat{w}_x^2 - \hat{w}_y^2) \cos I \sin 2\Omega \sin 2\omega \right] - \end{aligned}$$

$$\begin{aligned}
& - \frac{4e^2 \tan\left(\frac{I}{2}\right)}{\sqrt{1-e^2}} [\hat{w}_z \cos I - \sin I (\hat{w}_y \cos \Omega - \hat{w}_x \sin \Omega)] \cdot \\
& \cdot \left[\hat{w}_z \left(e^2 + \left(-2 + e^2 + 2\sqrt{1-e^2} \right) \cos 2\omega \right) \sin I + \right. \\
& + \cos I \left(e^2 + \left(-2 + e^2 + 2\sqrt{1-e^2} \right) \cos 2\omega \right) (\hat{w}_y \cos \Omega - \hat{w}_x \sin \Omega) - \\
& \left. - \left(-2 + e^2 + 2\sqrt{1-e^2} \right) (\hat{w}_x \cos \Omega + \hat{w}_y \sin \Omega) \sin 2\omega \right] \}. \quad (\text{B.15})
\end{aligned}$$

In the limit $e \rightarrow 0$, the leading terms in eq. (B.12)-eq. (B.15) are of order $\mathcal{O}(e^0)$. The next non-vanishing terms are of order $\mathcal{O}(e^2)$ for all the elements, with the exception of e whose next-to-leading order term is of order $\mathcal{O}(e)$.

B.3 The $v_r w_r$ term

The mixed term of eq. (16), proportional to Δm , causes non-vanishing long-term changes for all the orbital elements, apart from a . They are formally identical to those in Appendix A.3 with α_1 replaced by α_2 since it turned out that $\langle \tilde{\mathcal{H}}_{\alpha_2}^{\Delta m} \rangle$ is identical to $\langle \mathcal{H}_{\alpha_1}^{\Delta m} \rangle$ in eq. (A.4). Thus, Δm does not contribute to the overall orbital perturbations due to α_2 because the precessions coming from the Δm term in eq. (16) are canceled by those coming from the Δm term in the first piece of eq. (15).

The total α_2 -induced precessions are made up of the $(w/c)^2$ terms of Appendix B.2, proportional to $a^{-3/2}$, and of the terms containing the product of the masses which are completely negligible in the Solar System. In the case of a tight binary pulsar with, say, $m_A \approx m_B \approx M/2$, $a \approx 9.0 \times 10^5$ km, the precessions of Appendix A.1, rescaled by $-\alpha_2/\alpha_1$, and Appendix B.1 are proportional to $(v_{\text{orb}}/c)^2$, with $v_{\text{orb}} \approx 600$ km s $^{-1}$; for typical values of w (see Section 4), they are dominant with respect to the precessions of Appendix B.2.

References

- [1] T. Kibble, ‘‘Lorentz invariance and the gravitational field,’’ *Journal of Mathematical Physics* **2** no. 2, (March, 1961) 212–222.

- [2] V. A. Kostelecký and N. Russell, “Data tables for Lorentz and CPT violation,” *Reviews of Modern Physics* **83** no. 1, (Jan., 2011) 11–32, [arXiv:0801.0287 \[hep-ph\]](#).
- [3] C. M. Will, *Theory and Experiment in Gravitational Physics*. Cambridge University Press, Mar., 1993.
- [4] C. Will, “The Confrontation between General Relativity and Experiment,” *Living Reviews in Relativity* **9** no. 3, (2006) , <http://www.livingreviews.org/lrr-2006-3>.
- [5] D. Mattingly, “Modern Tests of Lorentz Invariance,” *Living Reviews in Relativity* **8** (Sept., 2005) 5, [arXiv:gr-qc/0502097](#).
- [6] S. Capozziello and V. Faraoni, *Beyond Einstein Gravity: A Survey of Gravitational Theories for Cosmology and Astrophysics*, vol. 170 of *Fundamental Theories of Physics*. Springer, Berlin, 2011.
- [7] T. Clifton, P. G. Ferreira, A. Padilla, and C. Skordis, “Modified gravity and cosmology,” *Physics Reports* **513** no. 1, (Mar., 2012) 1–189, [arXiv:1106.2476 \[astro-ph.CO\]](#).
- [8] C. M. Will and K. Nordtvedt, Jr., “Conservation Laws and Preferred Frames in Relativistic Gravity. I. Preferred-Frame Theories and an Extended PPN Formalism,” *The Astrophysical Journal* **177** (Nov., 1972) 757–774.
- [9] J. D. Bekenstein, “Relativistic gravitation theory for the modified Newtonian dynamics paradigm,” *Physical Review D* **70** no. 8, (Oct., 2004) 083509, [arXiv:astro-ph/0403694](#).
- [10] T. Jacobson and D. Mattingly, “Gravity with a dynamical preferred frame,” *Physical Review D* **64** no. 2, (July, 2001) 024028, [arXiv:gr-qc/0007031](#).
- [11] C. Heinicke, P. Baekler, and F. W. Hehl, “Einstein-aether theory, violation of Lorentz invariance, and metric-affine gravity,” *Physical Review D* **72** no. 2, (July, 2005) 025012, [arXiv:gr-qc/0504005](#).

- [12] T. Jacobson, “Einstein-æther gravity: a status report,” in *From Quantum to Emergent Gravity: Theory and Phenomenology*, vol. PoS (QG-Ph) 020. SISSA, 2007.
- [13] T. G. Zlosnik, P. G. Ferreira, and G. D. Starkman, “Modifying gravity with the aether: An alternative to dark matter,” *Physical Review D* **75** no. 4, (Feb., 2007) 044017, [arXiv:astro-ph/0607411](#).
- [14] X.-H. Meng and X.-L. Du, “A Specific Case of Generalized Einstein-aether Theories,” *Communications in Theoretical Physics* **57** no. 2, (Feb., 2012) 227–233, [arXiv:1109.0823 \[astro-ph.CO\]](#).
- [15] J. Bekenstein, “The modified Newtonian dynamics - MOND and its implications for new physics,” *Contemporary Physics* **47** no. 6, (Nov., 2006) 387–403, [arXiv:astro-ph/0701848](#).
- [16] J.-P. Bruneton and G. Esposito-Farèse, “Field-theoretical formulations of MOND-like gravity,” *Physical Review D* **76** no. 12, (Dec., 2007) 124012.
- [17] R. H. Sanders, “Hiding Lorentz invariance violation with MOND,” *Physical Review D* **84** no. 8, (Oct., 2011) 084024, [arXiv:1105.3910 \[gr-qc\]](#).
- [18] B. Famaey and S. S. McGaugh, “Modified Newtonian Dynamics (MOND): Observational Phenomenology and Relativistic Extensions,” *Living Reviews in Relativity* **15** (Sept., 2012) 10, [arXiv:1112.3960 \[astro-ph.CO\]](#).
- [19] P. Hořava, “Quantum gravity at a Lifshitz point,” *Physical Review D* **79** no. 8, (Apr., 2009) 084008, [arXiv:0901.3775 \[hep-th\]](#).
- [20] P. Hořava, “Membranes at quantum criticality,” *Journal of High Energy Physics* **3** (Mar., 2009) 20, [arXiv:0812.4287 \[hep-th\]](#).
- [21] T. Jacobson, “Extended Hořava gravity and Einstein-aether theory,” *Physical Review D* **81** no. 10, (May, 2010) 101502.

- [22] T. P. Sotiriou, “Hořava-Lifshitz gravity: a status report,”
Journal of Physics Conference Series **283** no. 1, (Feb., 2011) 012034,
arXiv:1010.3218 [hep-th].
- [23] M. Pospelov and Y. Shang, “Lorentz violation in Hořava-Lifshitz-type theories,” *Physical Review D* **85** no. 10, (May, 2012) 105001,
arXiv:1010.5249 [hep-th].
- [24] S. G. Nibbelink and M. Pospelov, “Lorentz Violation in Supersymmetric Field Theories,”
Physical Review Letters **94** no. 8, (Mar., 2005) 081601,
arXiv:hep-ph/0404271.
- [25] O. Pujolàs and S. Sibiryakov, “Supersymmetric aether,”
Journal of High Energy Physics **1** (Jan., 2012) 62,
arXiv:1109.4495 [hep-th].
- [26] V. A. Kostelecký, “Gravity, Lorentz violation, and the standard model,” *Physical Review D* **69** no. 10, (May, 2004) 105009,
arXiv:hep-th/0312310.
- [27] Q. G. Bailey and V. A. Kostelecký, “Signals for Lorentz violation in post-Newtonian gravity,”
Physical Review D **74** no. 4, (Aug., 2006) 045001,
arXiv:gr-qc/0603030.
- [28] G. Lambiase, “Standard Model extension with gravity and gravitational baryogenesis,”
Physics Letters B **642** no. 1-2, (Nov., 2006) 9–12,
arXiv:hep-ph/0612212.
- [29] Q. G. Bailey, “Lorentz-violating gravitoelectromagnetism,”
Physical Review D **82** no. 6, (Sept., 2010) 065012,
arXiv:1005.1435 [gr-qc].
- [30] V. A. Kostelecký and J. D. Tasson, “Matter-gravity couplings and Lorentz violation,” *Physical Review D* **83** no. 1, (Jan., 2011) 016013,
arXiv:1006.4106 [gr-qc].
- [31] I. H. Stairs, A. J. Faulkner, A. G. Lyne, M. Kramer, D. R. Lorimer, M. A. McLaughlin, R. N. Manchester, G. B. Hobbs, F. Camilo, A. Possenti, M. Burgay, N. D’Amico, P. C. Freire, and P. C. Gregory, “Discovery of Three Wide-Orbit Binary Pulsars: Implications for

- Binary Evolution and Equivalence Principles,”
The Astrophysical Journal **632** no. 2, (Oct., 2005) 1060–1068,
 arXiv:astro-ph/0506188.
- [32] A. Milani, D. Vokrouhlický, D. Villani, C. Bonanno, and A. Rossi,
 “Testing general relativity with the BepiColombo radio science
 experiment,” *Physical Review D* **66** no. 8, (Oct., 2002) 082001.
- [33] N. Ashby, P. L. Bender, and J. M. Wahr, “Future gravitational
 physics tests from ranging to the BepiColombo Mercury planetary
 orbiter,” *Physical Review D* **75** no. 2, (Jan., 2007) 022001.
- [34] K. Nordtvedt, “A post-Newtonian gravitational Lagrangian formalism
 for celestial body dynamics in metric gravity,”
The Astrophysical Journal **297** (Oct., 1985) 390–404.
- [35] K. Nordtvedt, “Probing gravity to the second post-Newtonian order
 and to one part in 10 to the 7th using the spin axis of the sun,”
The Astrophysical Journal **320** (Sept., 1987) 871–874.
- [36] T. Damour and G. Esposito-Farèse, “Testing local Lorentz invariance
 of gravity with binary-pulsar data,”
Physical Review D **46** no. 10, (Nov., 1992) 4128–4132.
- [37] L. Shao and N. Wex, “New tests of local Lorentz invariance of gravity
 with small-eccentricity binary pulsars,”
Classical and Quantum Gravity **29** no. 21, (Oct., 2012) 215018,
 arXiv:1209.4503 [gr-qc].
- [38] A. Verma, A. Fienga, J. Laskar, H. Manche, and M. Gastineau, “Use
 of MESSENGER radioscience data to improve planetary ephemeris
 and to test general relativity,” *arXiv:1306.5569 [astro-ph.EP]* (June,
 2013), arXiv:1306.5569 [astro-ph.EP].
- [39] M. Efroimsky and P. Goldreich, “Gauge freedom in the N-body
 problem of celestial mechanics,”
Astronomy & Astrophysics **415** (Mar., 2004) 1187–1199,
 arXiv:astro-ph/0307130.
- [40] M. Efroimsky, “Long-Term Evolution of Orbits About A Precessing
 Oblate Planet: 1. The Case of Uniform Precession,”
Celestial Mechanics and Dynamical Astronomy **91** no. 1-2, (Jan., 2005) 75–108,
 arXiv:astro-ph/0408168.

- [41] S. Kopeikin, M. Efroimsky, and G. Kaplan, *Relativistic Celestial Mechanics of the Solar System*. Wiley-VCH, Berlin, Sept., 2011.
- [42] B. Bertotti, P. Farinella, and D. Vokrouhlický, *Physics of the Solar System*. Kluwer Academic Press, Dordrecht, 2003.
- [43] M. Capderou, *Satellites. Orbits and Missions*. Springer-Verlag France, Paris, 2005.
- [44] M. Calura, P. Fortini, and E. Montanari, “Post-Newtonian Lagrangian planetary equations,” *Physical Review D* **56** no. 8, (Oct., 1997) 4782–4788, [arXiv:gr-qc/9708057](#).
- [45] M. Calura, E. Montanari, and P. Fortini, “Lagrangian planetary equations in Schwarzschild spacetime,” *Classical and Quantum Gravity* **15** no. 10, (Oct., 1998) 3121–3129, [arXiv:gr-qc/9807007](#).
- [46] V. A. Brumberg, L. S. Evdokimova, and N. G. Kochina, “Analytical Methods for the Orbits of Artificial Satellites of the Moon,” *Celestial Mechanics* **3** no. 2, (June, 1971) 197–221.
- [47] M. Efroimsky, “Gauge Freedom in Orbital Mechanics,” *Annals of the New York Academy of Sciences* **1065** no. 1, (Dec., 2005) 346–374, [arXiv:astro-ph/0603092](#).
- [48] T. Damour and G. Esposito-Farèse, “Testing for preferred-frame effects in gravity with artificial Earth satellites,” *Physical Review D* **49** no. 4, (Feb., 1994) 1693–1706, [arXiv:gr-qc/9311034](#).
- [49] A. Fienga, J. Laskar, P. Kuchynka, H. Manche, G. Desvignes, M. Gastineau, I. Cognard, and G. Theureau, “The INPOP10a planetary ephemeris and its applications in fundamental physics,” *Celestial Mechanics and Dynamical Astronomy* **111** no. 3, (Nov., 2011) 363–385, [arXiv:1108.5546 \[astro-ph.EP\]](#).
- [50] P. C. C. Freire, C. G. Bassa, N. Wex, I. H. Stairs, D. J. Champion, S. M. Ransom, P. Lazarus, V. M. Kaspi, J. W. T. Hessels, M. Kramer, J. M. Cordes, J. P. W. Verbiest, P. Podsiadlowski, D. J. Nice, J. S. Deneva, D. R. Lorimer, B. W. Stappers, M. A. McLaughlin, and F. Camilo,

- “On the nature and evolution of the unique binary pulsar J1903+0327,”
Monthly Notices of the Royal Astronomical Society **412** no. 4, (Apr., 2011) 2763–2780,
 arXiv:1011.5809 [astro-ph.GA].
- [51] P. C. C. Freire, M. Kramer, and N. Wex, “Tests of the universality of free fall for strongly self-gravitating bodies with radio pulsars,”
Classical and Quantum Gravity **29** no. 18, (Sept., 2012) 184007,
 arXiv:1205.3751 [gr-qc].
- [52] S. Kopeikin, “On possible implications of orbital parallaxes of wide orbit binary pulsars and their measurability,” *The Astrophysical Journal* **439** (January, 1995) L5–L8.
- [53] S. Kopeikin, “Proper motion of binary pulsars as a source of secular variations of orbital parameters,” *The Astrophysical Journal* **467** (August, 1996) L93–L95.
- [54] W. van Straten, M. Bailes, M. Britton, S. R. Kulkarni, S. B. Anderson, R. N. Manchester, and J. Sarkissian, “A test of general relativity from the three-dimensional orbital geometry of a binary pulsar,” *Nature* **412** no. 6843, (July, 2001) 158–160.
- [55] K. Nordtvedt, Jr. and C. M. Will, “Conservation Laws and Preferred Frames in Relativistic Gravity. II. Experimental Evidence to Rule Out Preferred-Frame Theories of Gravity,”
The Astrophysical Journal **177** (Nov., 1972) 775–792.
- [56] N. Wex and M. Kramer, “A characteristic observable signature of preferred-frame effects in relativistic binary pulsars,”
Monthly Notices of the Royal Astronomical Society **380** no. 9, (Sept., 2007) 455–465,
 arXiv:0706.2382.
- [57] G. Hinshaw, J. L. Weiland, R. S. Hill, N. Odegard, D. Larson, C. L. Bennett, J. Dunkley, B. Gold, M. R. Greason, N. Jarosik, E. Komatsu, M. R. Nolta, L. Page, D. N. Spergel, E. Wollack, M. Halpern, A. Kogut, M. Limon, S. S. Meyer, G. S. Tucker, and E. L. Wright, “Five-Year Wilkinson Microwave Anisotropy Probe Observations: Data Processing, Sky Maps, and Basic Results,”
The Astrophysical Journal Supplement **180** no. 2, (Feb., 2009) 225–245,
 arXiv:0803.0732.

- [58] T. Damour and G. Esposito-Farese, “Nonperturbative strong-field effects in tensor-scalar theories of gravitation,” *Physical Review Letters* **70** no. 15, (Apr., 1993) 2220–2223.
- [59] R. W. Hellings, “Testing relativity with solar system dynamics,” in *General Relativity and Gravitation Conference*, B. Bertotti, F. de Felice, and A. Pascolini, eds., pp. 365–385. Reidel, Dordrecht, 1984.
- [60] J. Müller, J. Williams, and S. Turyshev, “Lasers, clocks and drag-free control,” in *Lunar Laser Ranging Contributions to Relativity and Geodesy*, H. Dittus, C. Lämmerzahl, and S. Turyshev, eds., vol. 349 of *Astrophysics and Space Science Library*, pp. 457–472. Springer Verlag, 2008.
- [61] N. Wex, “Small-eccentricity binary pulsars and relativistic gravity,” in *IAU Colloq. 177: Pulsar Astronomy - 2000 and Beyond*, M. Kramer, N. Wex, and R. Wielebinski, eds., vol. 202 of *Astronomical Society of the Pacific Conference Series*, pp. 113–116. 2000.
arXiv:gr-qc/0002032.
- [62] J. Antoniadis, M. H. van Kerkwijk, D. Koester, P. C. C. Freire, N. Wex, T. M. Tauris, M. Kramer, and C. G. Bassa, “The relativistic pulsar-white dwarf binary PSR J1738+0333 - I. Mass determination and evolutionary history,” *Monthly Notices of the Royal Astronomical Society* **423** no. 4, (July, 2012) 3316–3327, arXiv:1204.3948 [astro-ph.HE].
- [63] D. Souami and J. Souchay, “The solar system’s invariable plane,” *Astronomy & Astrophysics* **543** (July, 2012) A133.
- [64] P. K. Seidelmann, B. A. Archinal, M. F. A’Hearn, A. Conrad, G. J. Consolmagno, D. Hestroffer, J. L. Hilton, G. A. Krasinsky, G. Neumann, J. Oberst, P. Stooke, E. F. Tedesco, D. J. Tholen, P. C. Thomas, and I. P. Williams, “Report of the IAU/IAG Working Group on cartographic coordinates and rotational elements: 2006,” *Celestial Mechanics and Dynamical Astronomy* **98** no. 3, (July, 2007) 155–180.
- [65] R. Carrington, *Observations of the Spots on the Sun from November 9, 1853, to March 24, 1861, Made at Redhill*. Williams & Norgate, London, 1863.
- [66] *The Astronomical Almanac for the Year 2013*. United Kingdom Hydrographic Office, 2012.

- [67] J. G. Beck and P. Giles, “Helioseismic Determination of the Solar Rotation Axis,”
The Astrophysical Journal Letters **621** no. 2, (Mar., 2005) L153–L156.
- [68] L. Iorio, “Constraining the angular momentum of the Sun with planetary orbital motions and general relativity,”
Solar Physics **281** no. 2, (December, 2012) 815–826,
arXiv:1112.4168 [gr-qc].
- [69] R. J. Warburton and J. M. Goodkind, “Search for evidence of a preferred reference frame,”
The Astrophysical Journal **208** (Sept., 1976) 881–886.
- [70] C. Lange, F. Camilo, N. Wex, M. Kramer, D. C. Backer, A. G. Lyne, and O. Doroshenko, “Precision timing measurements of PSR J1012+5307,”
Monthly Notices of the Royal Astronomical Society **326** no. 1, (Sept., 2001) 274–282,
arXiv:astro-ph/0102309.
- [71] M. Burgay, N. D’Amico, A. Possenti, R. N. Manchester, A. G. Lyne, B. C. Joshi, M. A. McLaughlin, M. Kramer, J. M. Sarkissian, F. Camilo, V. Kalogera, C. Kim, and D. R. Lorimer, “An increased estimate of the merger rate of double neutron stars from observations of a highly relativistic system,”
Nature **426** no. 6966, (Dec., 2003) 531–533,
arXiv:astro-ph/0312071.
- [72] A. Fienga, H. Manche, J. Laskar, M. Gastineau, and A. Verma, “INPOP new release: INPOP10e,” *ArXiv e-prints* (Jan., 2013) ,
arXiv:1301.1510 [astro-ph.EP].
- [73] I. B. Khriplovich and E. V. Pitjeva, “Upper Limits on Density of Dark Matter in Solar System,”
International Journal of Modern Physics D **15** no. 4, (2006) 615–618,
arXiv:astro-ph/0601422.
- [74] N. Pitjev and E. Pitjeva, “Constraints on Dark Matter in the Solar System,” *Astronomy Letters* **39** no. 3, (March, 2013) 141–149.
- [75] L. Blanchet and J. Novak, “External field effect of modified Newtonian dynamics in the Solar system,”
Monthly Notices of the Royal Astronomical Society **412** (Apr., 2011) 2530–2542,
arXiv:1010.1349 [astro-ph.CO].

- [76] M. Sereno and P. Jetzer, “Dark matter versus modifications of the gravitational inverse-square law: results from planetary motion in the Solar system,”
Monthly Notices of the Royal Astronomical Society **371** no. 2, (Sept., 2006) 626–632,
arXiv:astro-ph/0606197.
- [77] J. D. Anderson, P. A. Laing, E. L. Lau, A. S. Liu, M. M. Nieto, and S. G. Turyshev, “Indication, from Pioneer 10/11, Galileo, and Ulysses Data, of an Apparent Anomalous, Weak, Long-Range Acceleration,”
Physical Review Letters **81** (Oct., 1998) 2858–2861,
arXiv:gr-qc/9808081.
- [78] J. D. Anderson, P. A. Laing, E. L. Lau, A. S. Liu, M. M. Nieto, and S. G. Turyshev, “Study of the anomalous acceleration of Pioneer 10 and 11,” *Physical Review D* **65** no. 8, (Apr., 2002) 082004,
arXiv:gr-qc/0104064.
- [79] L. Iorio,
“The Lense-Thirring Effect and the Pioneer Anomaly: Solar System Tests,”
in *The Eleventh Marcel Grossmann Meeting On Recent Developments in Theoretical and Experimental General Relativity, Gravitation and Relativistic Field Theories*, H. Kleinert, R. T. Jantzen, and R. Ruffini, eds., pp. 2558–2560. Sept., 2008. arXiv:gr-qc/0608105.
- [80] E. M. Standish,
“Planetary and Lunar Ephemerides: testing alternate gravitational theories,”
in *Recent Developments in Gravitation and Cosmology*, A. Macias, C. Lämmerzahl, and A. Camacho, eds., vol. 977 of *American Institute of Physics Conference Series*, pp. 254–263. Mar., 2008.
- [81] A. Fienga, J. Laskar, P. Kuchynka, H. Manche, M. Gastineau, and C. Le Poncin-Lafitte, “Gravity tests with INPOP planetary ephemerides,” in *SF2A-2009: Proceedings of the Annual meeting of the French Society of Astronomy and Astrophysics*, M. Heydari-Malayeri, C. Reyl’E, and R. Samadi, eds., pp. 105–109. Société Française d’Astronomie & d’Astrophysique, Nov., 2009.
- [82] E. M. Standish, “Testing alternate gravitational theories,” in *IAU Symposium*, S. A. Klioner, P. K. Seidelmann, and M. H. Soffel, eds., vol. 261 of *IAU Symposium*, pp. 179–182. Cambridge University Press, Cambridge, Jan., 2010.

- [83] A. Fienga, J. Laskar, A. Verma, H. Manche, and M. Gastineau, “INPOP: Evolution, applications, and perspective,” in *SF2A-2012: Proceedings of the Annual meeting of the French Society of Astronomy and Astrophysics*, S. Boissier, P. de Laverny, N. Nardetto, R. Samadi, D. Valls-Gabaud, and H. Wozniak, eds., pp. 25–33. Société Française d’Astronomie & d’Astrophysique, Dec., 2012.
- [84] W. M. Folkner, “Relativistic Aspects of the JPL Planetary Ephemeris,” in *IAU Symposium*, S. A. Klioner, P. K. Seidelmann, and M. H. Soffel, eds., vol. 261 of *IAU Symposium*, pp. 155–158. Cambridge University Press, Cambridge, Jan., 2010.
- [85] L. Iorio, “Solar system constraints on a Rindler-type extra-acceleration from modified gravity at large distances,” *Journal of Cosmology and Astroparticle Physics* **5** (May, 2011) 19, [arXiv:1012.0226 \[gr-qc\]](#).
- [86] A. Hees, B. Lamine, S. Reynaud, M.-T. Jaekel, C. Le Poncin-Lafitte, V. Lainey, A. Füzfa, J.-M. Courty, V. Dehant, and P. Wolf, “Radioscience simulations in general relativity and in alternative theories of gravity,” *Classical and Quantum Gravity* **29** no. 23, (Dec., 2012) 235027, [arXiv:1201.5041 \[gr-qc\]](#).
- [87] U.-J. Le Verrier, “Lettre de M. Le Verrier à M. Faye sur la Théorie de Mercure et sur le Mouvement du Périhélie de cette Planète,” *Comptes rendus hebdomadaires des séances de l’Académie des sciences* **49** (July-december, 1859) 379–383.
- [88] A. Einstein, “Erklärung der Perihelbewegung des Merkur aus der allgemeinen Relativitätstheorie,” *Sitzungsber. Preuss. Akad. Wiss.* **47** (1915) 831–839.
- [89] J. Lense and H. Thirring, “Über den Einfluß der Eigenrotation der Zentralkörper auf die Bewegung der Planeten und Monde nach der Einsteinschen Gravitationstheorie,” *Physikalische Zeitschrift* **19** (1918) 156–163.
- [90] J.-P. Rozelot and C. Damiani, “History of solar oblateness measurements and interpretation,” *European Physical Journal H* **36** no. 3, (Nov., 2011) 407–436.

- [91] L. Iorio, “On the possibility of measuring the solar oblateness and some relativistic effects from planetary ranging,”
Astronomy & Astrophysics **433** (Apr., 2005) 385–393,
arXiv:gr-qc/0406041.
- [92] L. Iorio, “Is it possible to measure the Lense-Thirring effect on the orbits of the planets in the gravitational field of the Sun?,”
Astronomy & Astrophysics **431** (Feb., 2005) 385–389,
arXiv:gr-qc/0407047.
- [93] L. Iorio, “Perturbed stellar motions around the rotating black hole in Sgr A* for a generic orientation of its spin axis,”
Physical Review D **84** no. 12, (Dec., 2011) 124001.
- [94] S. C. Solomon, R. L. McNutt, R. E. Gold, and D. L. Domingue,
“MESSENGER Mission Overview,”
Space Science Reviews **131** no. 1-4, (Aug., 2007) 3–39.
- [95] J. Benkhoff, J. van Casteren, H. Hayakawa, M. Fujimoto, H. Laakso, M. Novara, P. Ferri, H. R. Middleton, and R. Ziethe,
“BepiColombo-Comprehensive exploration of Mercury: Mission overview and science goals,”
Planetary and Space Science **58** no. 1-2, (Jan., 2010) 2–20.
- [96] L. Iess, S. Asmar, and P. Tortora, “MORE: An advanced tracking experiment for the exploration of Mercury with the mission BepiColombo,” *Acta Astronautica* **65** no. 5-6, (Sept., 2009) 666–675.
- [97] L. Iess and S. Asmar, “Probing Space-Time in the Solar System: from Cassini to Bepicolombo,”
International Journal of Modern Physics D **16** no. 12a, (2007) 2117–2126.